PERGAMON

International Journal of Heat and Mass Transfer 42 (1999) 3337–3350

International Journal of HEAT and MASS TRANSFER

Rayleigh–Bénard stability of a solidifying porous medium

C. Mackie[a], P. Desai[b,*], C. Meyers[c]

[a]Tulane University, School of Mechanical Engineering, New Orleans, LA 70118, USA
[b]Georgia Institute of Technology, School of Mechanical Engineering, Atlanta, GA 30332, USA
[c]North Carolina A&T, College of Engineering, Greensboro, NC 27411, USA

Received 17 February 1998; received in revised form 8 October 1998

Abstract

In many solid/liquid phase transformation processes, natural convection controls the freezing or melting rate of the material. Freezing or melting in the presence of nonmelting components is important in numerous industrial processes and is also present in a wide range of systems in nature. The kinematics of the solid–liquid interface, coupled with bulk convection in the melt, play an important role in determining the microstructure of a solidified material. The fundamental problem of thermoconvective instability of a single-component fluid in a horizontal porous layer has been studied extensively; additional complexities arise during solidification due to the presence of a non-melting component, namely the porous medium. This study addresses the problem of Rayleigh–Bénard instability of a liquid layer undergoing a phase transformation within a porous medium. A linear stability analysis is performed to determine the effects of the medium and phase-change on the conditions for incipient instability under a range of thermal boundary conditions. The analysis reveals that the onset of convection, or the stability of the system, is significantly affected by the presence of the porous medium, state of solidification and the thermal boundary conditions.

1. Introduction

The problem of thermoconvective instability in a horizontal fluid layer driven by buoyancy effects studied extensively in the literature [1–3] encompasses unresolved complexities associated with the freezing or melting of a liquid in the presence of a nonmelting component, such as a solid matrix or soil. This study addresses hydrodynamic stability issues during solidification of such mixtures by modeling the matrix–liquid slurry as a liquid saturated horizontal porous medium in a gravitational field going through a phase change under a full range of thermal conditions at the lower bounding surface. Freezing or melting in the presence of nonmelting components is important in industrial applications as well as in a wide range of systems in nature. Examples include, but are not limited to, seasonal freezing and melting of soil, lakes and rivers, artificial freezing of the ground as a construction technique for supporting poor soils, insulation of underground buildings, the melting of the upper permafrost in the Arctic due to buried pipelines, thermal energy storage in porous media and storage of frozen foods. Metallurgical applications include manufacturing of composite materials and purification of metals. The study of freezing and melting in porous media has gained a great interest over the past few years. A fundamental understanding of convective stability in such a range of applications is thus very important.

It is recognized that fluid flow, in general, and buoyancy-driven flow, in particular, plays a critical role in determining interfacial traits of a solidifying material;

* Corresponding author. Tel: +1-404-894-3233; fax: +1 404-894-7790.
E-mail address: prateen.desai@me.gatech.edu (P. Desai)

0017-9310/99/$ - see front matter
PII: S0017-9310(98)00361-5

Nomenclature

a	separation constant or wave number
a_c	critical wave number
A	solid thickness ratio
B_L	Biot number, $h_\infty \eta_0 / k_L$
c_a	acceleration coefficient
c_i	general constants for characteristic equation
c_p	specific heat at constant pressure
D	differential operator, $D = \mathrm{d}/\mathrm{d}z$, $D^2 = \mathrm{d}^2/\mathrm{d}z^2$
Da	Darcy number, K/η_0^2
f	temperature perturbation variable (liquid), see Eq. (33)
g	temperature perturbation variable (solid), see Eq. (33)
$\boldsymbol{g}$	gravitational acceleration vector
h_{SL}	specific latent heat of solid
h_∞	heat transfer coefficient of the bulk environment
$\hat{k}$, $\hat{z}$	unit vector in the z-direction
$k_{L,S}$	thermal conductivity for liquid and solid, respectively
K	permeability of the porous medium
L	length of the solidification system
$\boldsymbol{n}$, $\hat{t}_i$	unit normal and tangent vectors
Pr	Prandtl number, ν_L/α_L
Ra	Rayleigh number, $g\beta(T_L - T_M)\eta_0^3/\nu_L\alpha_L$
Ra_c (Rac)	critical Rayleigh–Darcy number, $R_c \cdot Da$
R_c (Rc)	critical Rayleigh number
St	Stefan number, $h_{SL}/c_p\Delta T_L$
T	temperature
T_1	upper plate temperature
T_{10}	lower plate temperature
T_M	interface melting temperature
$\mathbf{v}$	velocity vector for liquid, $\mathbf{v} = \mathbf{v}(u, v, w)$
w	velocity component in the z-direction for the liquid
$\hat{w}$	vertical velocity perturbation variable
z	spatial coordinate in vertical direction for liquid.

Greek symbols

α	ratio of the thermal diffusivities of the liquid and the solid, α_L/α_S
β	volumetric coefficient of thermal expansion
γ_a	acceleration coefficient, $c_a/\sigma_H\, Pr$
ΔT_L	temperature difference across the porous layer
η	interface position coordinate
η	normalized perturbation variable for the interface position
η_0	length of the liquid saturated porous region
η_t	time rate of change of the interface
μ	μ_{eff}/μ_L
μ_L	dynamic viscosity
ν_L	kinematic viscosity
ρ	ratio of the densities of the liquid and the solid, ρ_L/ρ_S
σ	real part of the complex growth rate [s]
σ_H	heat capacity ratio, see Eq. (3)
ϕ	medium porosity
Φ	pattern planform, where $\Phi = \Phi(x, y)$
∇^2	Laplacian operator
∇_H^2	2-D Laplacian operator, see Eq. (35).

Subscripts

eff	effective property for porous medium
L	liquid property or region
M	melting temperature
S	solid property or region
0	reference state
∞	bulk environment.

Superscripts

$\bar{}$	bar, basic state quantity
$'$	perturbation variable
$*$	normalized.

fluid motion adjacent to a solidifying interface affects the local thermal and solutal fields which control the geometric, dynamic and thermodynamic characteristics of the interface. For instance, convection during fabrication or solidification processing of metal matrix composites affects the distribution of particulates in the composites, in turn influencing the properties of the material. In the pure metal analog, independent of the solute diffusion, it is also known that the convective stability is affected by the density and presence of particulates as well as by the conductivity of the boundary. The porous medium model simulates the influences of a non-interacting matrix, coupled with a range of thermal conditions at the lower boundary, on the initiation and growth of bulk convection in a solidifying nonhomogeneous system. This study focuses on the effect of the permeability of a porous medium and phase change on the incipient convection in the interstitial liquid; by parametrically changing the permeability from that corresponding to a Darcy model of the flow through it to a vanishing one, an understanding is gained for the influence of volume fraction and its distribution on the critical conditions for convective stability of the interstitial fluid in porous media in the presence of solidification.

This work couples solidification dynamics with the thermal and hydrodynamic fields in a nonhomogeneous solidifying system via a Rayleigh–Bénard stability analysis. The porous medium is saturated with the liquid in all available pores, or the interparticle space of the medium, leaving no space for a vapor, gas, or other liquid within the medium

Since the pioneering work on the porous-medium analog of the Rayleigh–Bénard stability problem [4], the subject of phase-change in a porous medium has received increasing attention over the past two decades. While liquid/gas phase change in a saturated porous medium has received considerable attention, solid/liquid phase change in liquid-saturated porous medium has received considerably less attention. Such problems and their manifestation represent a relatively new area in the field of convection in porous media [5]. This study considers a horizontal, liquid saturated, porous medium undergoing solidification while being cooled uniformly from above. A recent study [6] examined the coupled effects on stability arising from thermal convection and solidification of a single-component liquid in a porous medium. The stability of the basic state of heat conduction and the stability of finite-amplitude convection in the Darcy limit of vanishing permeability for isothermal boundaries were examined via a two-parameter perturbation analysis. The present work investigates the effects of the solid matrix in a pure melt on the thermal convection for a range of permeabilities and the full range of lower wall thermal boundary conditions. The cited references are based on the Darcy flow model, and hence are relevant to well packed low permeability porous media. This study differs by including the Brinkman extended flow model that allows for the investigation of sparsely packed media.

Beyond the context of convective stability, there exists substantial research in porous media transport phenomena germane to the present work. Non-Darcian effects have been modeled illustrating the transition between the porous and clear fluid limits by modifying the Darcy equation with the Brinkman term [10]. Also experiments have been conducted using a modified Darcy equation incorporating the Forchheimer term which attempts to account for microscopic drag forces due to acceleration [11]. It was demonstrated experimentally [7] that an effective porous medium thermal conductivity model is adequate for heat transfer estimates only when the solid matrix and pore-material have sufficiently similar thermal conductivities to allow for the requisite local thermal equilibrium. A continuum model of the porous medium was developed [8] for analyzing solid/liquid phase

change in a porous medium that accounted for inertia as well as boundary friction effects. In particular, these include the Brinkman viscous and the Forchheimer pressure drag terms. Such results are relevant to the present work where the liquid and the porous material have similar conductivities, and where friction due to microscopic shear is also important.

2. The mathematical model

A quiescent horizontal layer of a pure fluid in a gravitational field heated from below does not always remain so in the presence of an adverse density gradient beyond a threshold value which is capable of giving rise to fluid motion. This observation may be applied to examine the solidification (or melting) of a porous layer saturated with a pure liquid enclosed between two rigid, parallel, thermally dissimilar, horizontal plates of infinite extent, a distance L apart, in a gravitational field, as shown in Fig. 1. The analytical model is formulated under the assumptions that the liquid in the upper part of the layer is frozen and the effective thermophysical and transport properties of the porous medium are homogeneous and isotropic. The porous matrix and the solidified layer are both assumed to be rigid [8]. Fluid motion within the porous medium is described via a Newtonian, Boussinesq model of the Navier–Stokes equations, written for a liquid saturated porous medium. Motion due to density change upon phase change is not considered to be significant. The liquid velocity through the medium is deemed sufficiently small, conforming to the Darcy regime, or, at most, to the Brinkman-modified Darcy regime. The melt–freeze front is assumed to be a thin surface of negligible thickness that remains at the melting point of the phase-change material. The fluid layer is separated at the bottom from the surroundings by a thin rigid lamina of negligible heat capacity. The upper plate is maintained at a constant temperature, T_1.

2.1. Governing equations

In the porous layer, the heat transfer at the lower surface of the system is via a convective–conductive mechanism. The flux at the bottom plate is maintained such that the melting temperature, T_M, is bounded between the lower plate temperature, T_{10}, and the upper plate temperature, T_1 ($T_{10} > T_M > T_1$). Therefore, there is a solid–liquid interface at $z = \eta_0$, $0 < \eta_0 < L$. The governing equations are written in a Cartesian frame fixed with respect to the composite system on the lower plate with the positive z-axis pointing

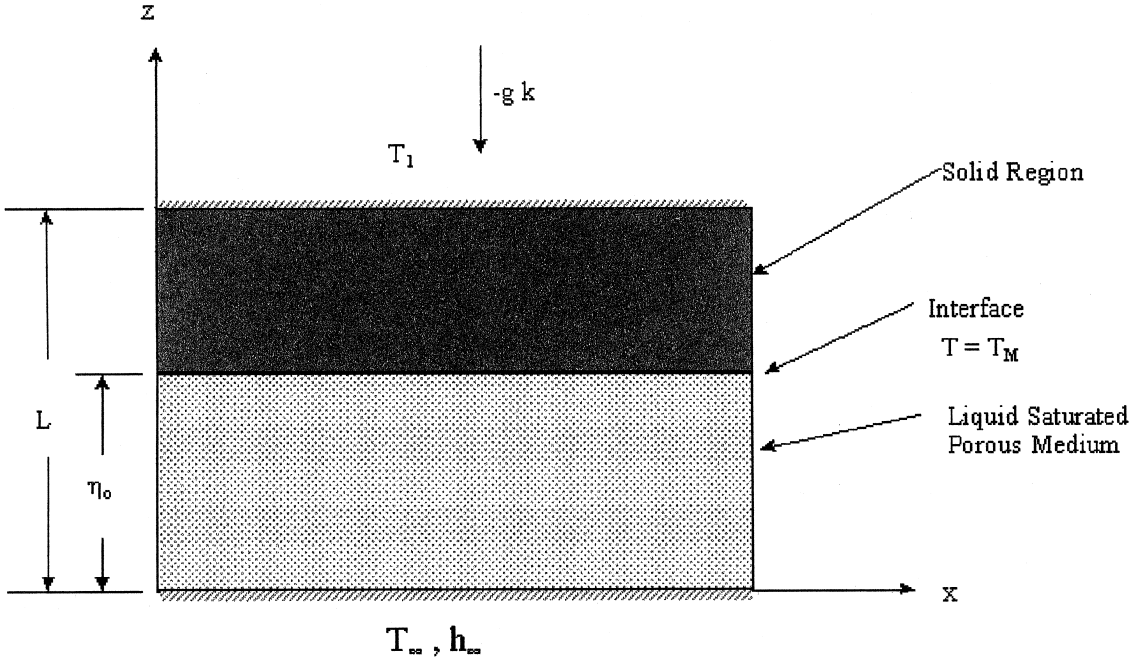

Fig. 1. Solidification model with saturated porous medium.

upward (see Fig. 1). The temperature field within the solidified layer is described by the thermal energy equation

$$\frac{\partial T_S}{\partial t} = \alpha_S \nabla^2 T_S. \tag{1}$$

For the liquid, the temperature field may be obtained from a simultaneous solution of the thermal energy and continuity equations, together with the Boussinesq model of the Darcy-extended momentum equation. These are expressed, respectively, as

$$\sigma_H \frac{\partial T_L}{\partial t} + \mathbf{v} \cdot \nabla T_L = \alpha_L \nabla^2 T_L \tag{2}$$

where

$$\sigma_H = \frac{\phi(\rho c_\rho)_L (1-\phi)(\rho c_\rho)_S}{(\rho c_\rho)_L} \equiv \text{heat capacity ratio} \tag{3}$$

$$\nabla \cdot \mathbf{v} = 0 \tag{4}$$

and

$$c_a \rho_L \frac{\partial \mathbf{v}}{\partial t} = -\nabla P - \left(\frac{\mu_L}{K}\right)\mathbf{v} + \mu_{\text{eff}} \nabla^2 \mathbf{v} + \rho_L \beta (T_L - T_{\text{ref}}) \mathbf{g} \hat{k} \tag{5}$$

where c_a is a constant which depends on the geometry of the porous medium and is determined by the nature of the assumed model pore tubes [5]. In most cases, the term becomes negligible when suitably scaled. This is due to the small value of permeability which multiplies the scaled inertia term.

In the proceeding governing equations, the Brinkman-extended Darcy momentum model is employed. The frictional effects represented by Darcy law in the fluid momentum equation in a porous medium, are two orders of magnitude lower than those represented in the Navier–Stokes equations. Thus, only the impermeability condition at the surface is satisfied, leaving the no-slip boundary condition unresolved. The Brinkman-extended Darcy model satisfies not only the impermeability and no-slip conditions but accounts also for the friction caused by microscopic shear by introducing an additional viscous force term via an effective dynamic viscosity, $\mu_{\text{eff}} \nabla^2 \mathbf{v}$. The Brinkman-extended model reduces to a form of the Navier–Stokes model as the medium permeability approach infinity ($K \to \infty$) and to the conventional Darcy model as the medium permeability approach zero ($K \to 0$). Such a formulation allows a comparison of the flows in porous media with those in clear fluids.

2.2. Boundary conditions

The boundary conditions at the phase boundary are the continuity of temperature

$$T_L = T_S = T_M \tag{6}$$

where the interface curvature due to undercooling of the melt is neglected, and the conservation of energy

$$\rho_S h_{SL} \frac{\partial \eta}{\partial t} = | k_S \nabla T_S - k_L \nabla T_L | \cdot \boldsymbol{n}. \tag{7}$$

Also defined on this boundary (interface) are the conservation of mass (the kinematic condition)

$$\rho_L (\mathbf{v} \cdot \boldsymbol{n}) = (\rho_L - \rho_S) \frac{\partial \eta}{\partial t} \boldsymbol{k} \cdot \boldsymbol{n} \tag{8}$$

and the no-slip condition

$$\mathbf{v} \cdot \boldsymbol{t}_1 = \mathbf{v} \cdot \boldsymbol{t}_2. \tag{9}$$

The boundary conditions on the two bounding surfaces are

$$\text{at } z = 0, \quad -k_L \left.\frac{dT_L}{dz}\right|_0 = h_\infty (T_\infty - T_{10}) \qquad \text{and at } z = L, \quad T_S = T_1. \tag{10}$$

3. Basic state and linear stability analysis

Initially, the stationary system is in a static equilibrium state with no fluid motion and a planar interface at $z = \eta_0$. The purely conductive temperature profiles in the liquid and the solid regions are, respectively, given by

$$T_L = \frac{-h_\infty (T_\infty - T_M) z}{h_\infty \eta_0 + k_L} + \frac{(T_\infty - T_M) h_\infty \eta_0}{h_\infty \eta_0 + k_L} + T_M \tag{11}$$

and

$$T_S = \frac{T_M - T_1}{\eta_0 - L} z - \frac{\eta_0 (T_M - T_1)}{\eta_0 - L} + T_M. \tag{12}$$

The static equilibrium temperature profiles are used to normalize the solid and liquid temperatures, respectively, as

$$T_L^* = \frac{T_L - T_M}{T_{10} | - T_M}; \quad T_s^* = \frac{T_S - T_1}{T_M - T_1}. \tag{13}$$

The scales for, v, x (and y, z), t and p are chosen, respectively, as

$$\frac{\alpha_L}{\eta_0},\eta_0,\frac{\sigma_H\eta_0^2}{\alpha_L} \quad \text{and} \quad \frac{\rho_L\nu_L\alpha_L}{\eta_0^2}.$$

The normalized equations become, after dropping the asterisks, for the solid,

$$\left(\frac{1}{\sigma_H}\right)\frac{\partial T_S}{\partial t} = \frac{\alpha_S}{\alpha_L}\nabla^2 T_S \tag{14}$$

and for the liquid,

$$\frac{\partial T_L}{\partial t} + \mathbf{v}\cdot\nabla T_L = \nabla^2 T_L, \quad \nabla\cdot\mathbf{v} = 0 \tag{15a,b}$$

and

$$\gamma_a\frac{\partial \mathbf{v}}{\partial t} + \nabla P + \left(\frac{1}{Da}\right)\mathbf{v} - \tilde{\mu}\nabla^2\mathbf{v} + Ra\, T_L\boldsymbol{k} = 0. \tag{16}$$

The normalized boundary conditions on the interface are

$$\mathbf{v}\cdot\boldsymbol{t}_1 = \frac{(1-\rho)}{\sigma_H}\eta_t\boldsymbol{k}\cdot\boldsymbol{n}, \quad \mathbf{v}_1\cdot\boldsymbol{t}_1 = \mathbf{v}_2\cdot\boldsymbol{t}_2 = 0 \tag{17a,b}$$

$$\rho\, St\, Pr\,\frac{\partial\eta}{\partial t} = (A\nabla T_L - \nabla T_S)\cdot\boldsymbol{n}, \quad \text{and} \quad T_L = T_S = 0. \tag{18a,b}$$

The surface boundary conditions become

$$\text{at } z = 0, \quad \frac{dT_L}{dz} = B_L T_L, \quad \text{and at } z = L, T_S = 1. \tag{19a,b}$$

It may be noted that the dimensionless group, B_L, acts like a Biot number for heat transfer from the bulk environment to the liquid. As B_L approaches zero, the boundary condition at the surface approaches that of an insulated surface; as B_L approaches infinity, the boundary condition approaches that of a constant surface temperature; also appearing is another dimensionless parameter:

$$A = \frac{L-\eta_0}{\eta_0} = \frac{k_S}{k_L}\frac{\Delta T_S}{\Delta T_L} \tag{20}$$

where $z=\eta_0$ is the position of the planar interface and $z=L$ is the thickness of the combined solid–liquid system. For a small A, A^{-1} may be considered the equivalent Biot number for heat transfer from the liquid to the solid; also, A measures the amount of solid present in the system [9].

The basic state under consideration is that of a stagnant layer of liquid, with a hydrostatic pressure distribution, and a purely conductive temperature distribution. In normalized form the basic state becomes (denoted by variables with bars on top)

$$\mathbf{v} = 0; \quad \frac{d\bar{p}}{dz} = Ra\,\bar{T}_L\boldsymbol{k} \tag{21}$$

and

$$\bar{T}_L = 1 - z; \quad \bar{T}_S = 1 - \frac{z-1}{L-1}. \tag{22}$$

It is noted that $\bar{T}_L$ and $\bar{T}_S$ are scaled by different reference lengths. Thus at $z=1$, the temperature for the solid and liquid regions (T_L and T_S) are equal to the melting temperature, T_M [Eq. (12)]. Next, a linear perturbation model of the system is developed by considering a slight change in temperature due to a slight melting of the solid. Such a problem is formulated by introducing perturbations of the basic state defined via a conventional barred-primed scheme of notations as

$$T_S = \bar{T}_S + T'_S, \quad T_L = \bar{T}_L + T'_L \tag{23}$$

$$v = v', \quad p = \bar{p} + p', \quad \eta = 1 + \eta'. \tag{24}$$

Introduction of the perturbation expressions, Eqs. (23) and (24), into the governing Eqs. (14)–(16), followed by linearization in the disturbance quantities, yields the perturbation model for the solid,

$$\left(\frac{1}{\sigma_H}\right)\frac{\partial T'_S}{\partial t} = \left(\frac{\alpha_S}{\alpha_L}\right)\nabla^2 T'_S \tag{25}$$

and for the liquid

$$\frac{\partial T'_L}{\partial t} = w' + \nabla^2 T'_L, \quad \nabla\cdot\mathbf{v}' = 0 \tag{26}$$

and

$$\gamma_a\frac{\partial\mathbf{v}'}{\partial t} + \nabla p' + \left(\frac{1}{Da}\right)\mathbf{v}' - \tilde{\mu}\nabla^2\mathbf{v}' + Ra\, T'_L k = 0 \tag{27}$$

where w' is the vertical component of the perturbation velocity $\mathbf{v}'$. The linearized boundary conditions for the perturbation model are

$$\text{at } z = 1, \qquad T'_S = -\eta'\frac{\partial\bar{T}_S}{\partial z}, \quad T'_L = -\eta'\frac{\partial\bar{T}_L}{\partial z} \tag{28}$$

$$\rho\, St\, Pr\left(\frac{\partial\eta'}{\partial t}\right) = A\frac{\partial T'_S}{\partial z} - \frac{\partial T'_L}{\partial z} \tag{29}$$

and

$$u' = (1-\rho)\left(\frac{\partial \eta}{\partial x}\right)', \quad v' = (1-\rho)\left(\frac{\partial \eta}{\partial y}\right)', \quad w' = (1-\rho)\frac{\partial \eta}{\partial t}. \tag{30}$$

The surface boundary conditions become

$$\text{at } z = 0, \quad \frac{\mathrm{d}T'_{\mathrm{L}}}{\mathrm{d}z} = B_{\mathrm{L}} T'_{\mathrm{L}}, \quad \text{and at } z = L, \quad T'_{\mathrm{S}} = 0. \tag{31}$$

The solution to the preceding set of equations results in a sufficient condition to ascertain the stability boundary of the liquid layer, as would be expected from the linear analysis.

The linear perturbation system, [Eqs. (25)–(31)], is examined to determine the critical and necessary conditions for incipient nonlinear convection. After eliminating the pressure from the liquid momentum equation [Eq. (27)] by taking its curl, the curl is taken again, yielding

$$\begin{aligned} &-\gamma_{\mathrm{a}} \frac{\partial}{\partial t}(\nabla^2 w) - \frac{1}{Da}\nabla^2 w + \nabla^2(\nabla^2 w) + Ra\, \nabla_{\mathrm{H}}^2 T_{\mathrm{L}} = 0 \\ &\frac{\partial T_{\mathrm{L}}}{\partial t} - w - \nabla^2 T_{\mathrm{L}} = 0 \\ &\nabla^2 T_{\mathrm{S}} = 0 \end{aligned} \tag{32}$$

where the primes have been dropped. Next, to find normal modes solution to the linear stability problem it is noted that the variables become separable under this assumption, yielding solutions of the form

$$\{T_{\mathrm{S}}, T_{\mathrm{L}}, w, \eta\} = \{g(z), f(z), \hat{w}, \hat{\eta}\}\, \mathrm{e}^{\sigma t} \Phi(x,y) \tag{33}$$

where the time constant, $\sigma = \sigma_r + i\sigma_i$, contains σ_r, the growth rate, and σ_i, the frequency of the disturbance, and Φ is the plan form function which determines the cellular structure of the fluid motion and satisfies the two-dimensional wave or membrane equation

$$\Phi_{xx} + \Phi_{yy} = -a^2 \Phi \tag{34}$$

or

$$\nabla_{\mathrm{H}}^2 \Phi + a^2 \Phi = 0, \quad \text{where } \nabla_{\mathrm{H}}^2 = \frac{\partial}{\partial x^2} + \frac{\partial}{\partial y^2}. \tag{35}$$

It may be noted that 'a' is the separation constant, mathematically, in addition to being the nondimensional overall wave number, physically.

Substitution of the normal mode into the linear perturbation model [Eq. (32)] results in the normal-mode disturbance equations for the solid

$$\sigma g = \frac{\alpha_{\mathrm{S}}}{\alpha_{\mathrm{L}}}(D^2 - a^2) g \tag{36}$$

and, for the liquid

$$\sigma f = \hat{w} + (D^2 - a^2) f \tag{37}$$

and

$$-\gamma_{\mathrm{a}} \sigma (D^2 - a^2)\hat{w} = \left(\frac{1}{Da}\right)(D^2 - a^2)\hat{w} - (D^2 - a^2)^2 \hat{w} + Ra\, a^2 f \tag{38}$$

where an ordinary differential operator, D, has been defined as

$$D = \frac{\mathrm{d}}{\mathrm{d}z} \quad \text{and} \quad D^2 = \frac{\mathrm{d}^2}{\mathrm{d}z^2}. \tag{39}$$

The boundary conditions transform as

$$g(L) = 0, \quad g(1) = \frac{\hat{\eta}}{A} \tag{40}$$

for the solid region, and

$$Df(1) = ADg(1) \quad \hat{w}(1) = 1 - \rho\sigma\eta \quad D\hat{w}(1) = 1 - \rho\sigma\eta \quad \hat{w}(0) = 0 \quad D\hat{w}(0) = 0 \quad Df(0) = B_{\mathrm{L}} f(0) \tag{41}$$

in the liquid region.

4. Solutions

4.1. Solid region solution

It is noticed that the general solution for the solidified layer may be obtained independent of the liquid equations, resulting in

$$g(z) = C_1 \sinh(az) + C_2 \cosh(az). \tag{42}$$

Use of the boundary conditions, [Eq. (41)], yields the temperature profile in the solid as

$$g(z) = \frac{-\eta \sinh(a(1 + A - z))}{A \sinh(aA)}. \tag{43}$$

It was necessary first to solve for the solid region, independent of the liquid region, in order to express all of the governing equations in the liquid region in terms of the temperature perturbation variable, f.

4.2. Liquid region solution

The first two (liquid momentum and energy) equations in Eq. (32) are combined, thus eliminating the vertical velocity component, forming a single-variable perturbation equation in terms of the normal mode perturbation temperature, f. The combined expression becomes

$$\left(-\gamma_a\sigma^2-\sigma\frac{1}{Da}\right)(D^2-a^2)f+\left(\gamma_a\sigma+\frac{1}{Da}+\tilde{\mu}\sigma\right)\times(D^2-a^2)^2f-\tilde{\mu}(D^2-a^2)^3f+Ra\,a^2f=0. \tag{44}$$

Next, it is assumed that the principle of exchange of stability is valid, or that all possible values of the growth rate allowable are real. The implication of σ being real is that the neutral or marginal stability curve is characterized by a growth rate, σ, of zero. Accordingly, the single-variable temperature perturbation equation for the liquid [Eq. (44)] reduces to a sixth-order, linear, homogeneous equation

$$(D^2-a^2)^3f-\left(\frac{1}{Da}\right)(D^2-a^2)^2f+Ra\,a^2f=0 \tag{45}$$

with six linear, homogeneous boundary conditions (determined by applying the solid solution) and evaluating the continuity and thermal energy equations at $z=(0, 1)$, given as

$$(D^2-a^2)f(0)=0,\quad (D^2-a^2)f(1)=0$$

$$D(D^2-a^2)f(0)=0,\quad D(D^2-a^2)f(1)=0$$

$$Df(0)=B_Lf(0)\quad\text{and}\quad Df(1)+a\,\mathrm{Coth}\,[aA]f(1)=0. \tag{46}$$

The linear, homogeneous, sixth-order system [Eqs. (45) and (46)] constitutes an eigenvalue problem. The system obviously has the trivial solution, $f=0$, for any values of a, B_L, Ra, and Da, but, in general, also possesses non-trivial solutions depending on an eigenvalue, say λ, and has a general solution obtained as a linear combination of six linearly independent solutions. In this case, a, B_L, and Da become fixed parameters, with Ra serving as the eigenvalue, producing non-trivial continuous solutions for the perturbation temperature eigenfunction, $f(z)$. Use of the six boundary conditions and the general solution, $f(z)$, yields six simultaneous linear equations. This defines the eigenvalue problem in which Ra serves as the eigenvalue for a particular set of values for a, B_L, Da and A. The critical Rayleigh number for the onset of convection has a corresponding critical wave number, both of which being the minimum values satisfying each value as an eigenvalue. The solution for the stability problem is obtained for given values of B_L, Da and A, by determining iteratively the lowest characteristic values of a and Ra.

5. Results and discussion

The linear stability analysis for the system in this work has two experimentally verifiable results: the critical temperature difference for the onset of convection and the corresponding critical wavelength. For a range of boundary conditions varying from a constant temperature to a constant heat flux, the incipient conditions for convection for a pure liquid solidifying in a porous medium are determined.

5.1. Effect of varying solid thickness and boundary conditions

Since the solid portion of the porous medium is typically held at temperatures below the melt temperature, initial freezing begins with the contact between the medium and the superheated liquid. Physically, the removal of the latent heat takes place rapidly, creating a thin coating on the porous medium, the degree to which the permeability is affected due to such a phenomenon being quite small. Therefore, any change in permeability will be due to the solidification of the interstitial fluid within the slightly coated matrix. In the model, cooled from above, and/or heated from below, solidification occurs only at the interface; interstitial solidification does not occur. Therefore, Figs. 2–8, the critical conditions for incipient convection at fixed permeabilities are noted.

As the solidified portion of the system grows, or as, the aspect ratio of the layer, A, increases for a set of fixed values of the Darcy number, Da, and the Biot number, B_L, the critical Rayleigh number of the system decreases, rendering the system less stable. It may be noted, for a system with no solidification ($A=0$), constant temperature boundary, $B_L=1000$, and a dense medium, $Da\leqslant 10^{-6}$, that the classical problem of convection in a porous medium between two infinite walls, the so-called 'Lapwood problem', and the solution of $Ra_c=4\pi^2=39.45$ are recovered. Departure from the classical problem of rigid boundaries was determined as a function of solid thickness and the results are designated on Figs. 2–7 as the Lapwood problem recovering the results of Karcher et al. Results for other conditions may be compared with those resulting from the modified classical Lapwood case. Figs. 2–4 illustrate the effect of the solid thickness ratio on the critical Rayleigh number for fixed permeability for different boundary conditions, compared to the modi-

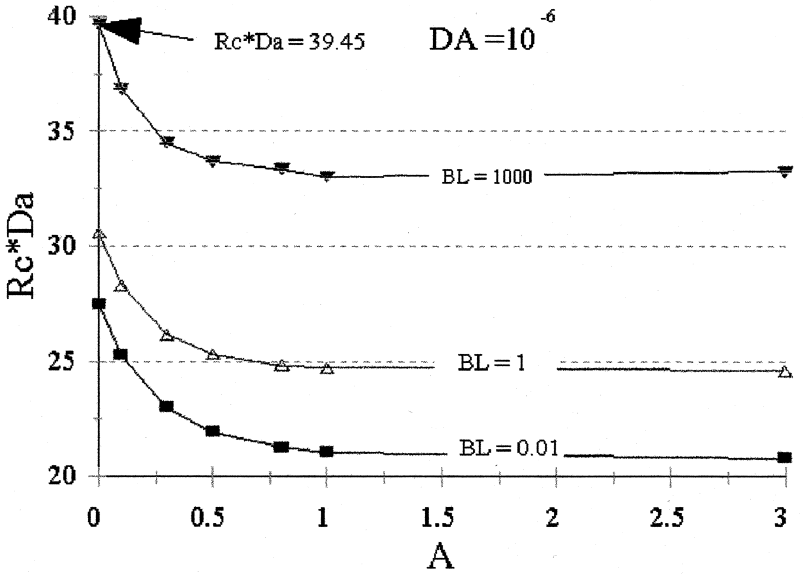

Fig. 2. Critical Rayleigh–Darcy number vs. solid thickness ratio for $Da = 10^{-6}$.

fied Lapwood solution, which is denoted by a thin dashed line. The figures also show that as the boundary condition at the bottom wall is modified from that of a fixed temperature ($B_L \to \infty$), to that of an insulated boundary ($B_L \to 0$), the system becomes less stable. For all values of the Darcy number considered, simultaneously increasing both the solid thickness ratio and the Biot number has a strictly stabilizing influence.

Figs. 2–7 indicate further that the critical Rayleigh–Darcy and wave numbers approach their lower limits asymptotically as $A \to \infty$. Such a destabilizing effect was previously documented for solidification in a bulk liquid-layer [9] as well as in a dense liquid saturated porous medium [6]. Considering the limiting case of an isothermal lower wall ($B_L = 1000$) and a densely packed medium ($Da = 10^{-6}$), there is a 16.44% decrease in the critical Rayleigh–Darcy number as the (normalized) solid thickness, A, increases monotonically from 0–∞;

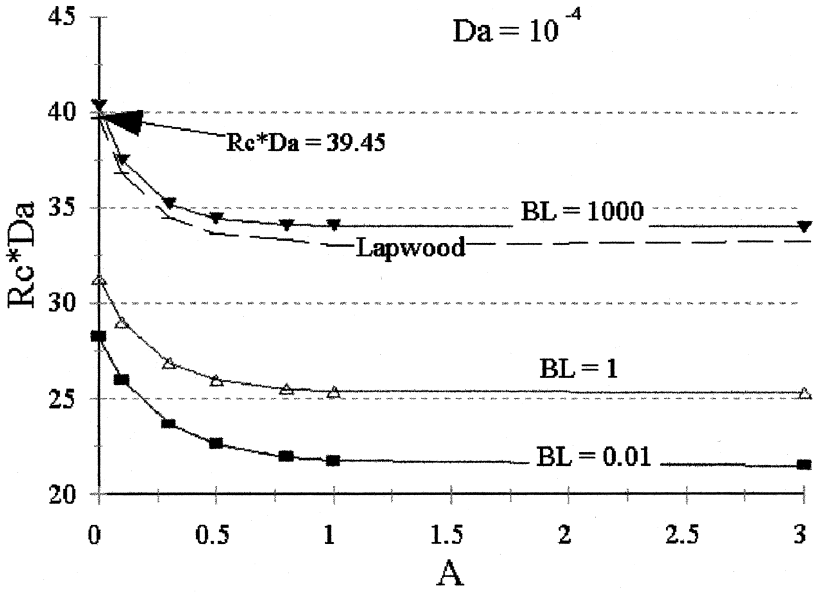

Fig. 3. Critical Rayleigh–Darcy number vs. solid thickness ratio for $Da = 10^{-4}$.

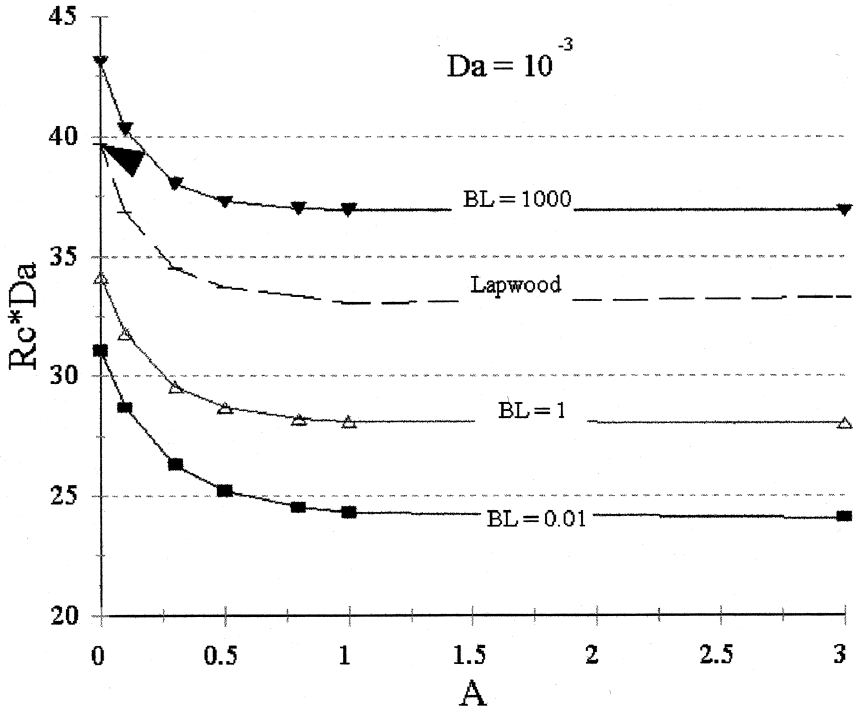

Fig. 4. Critical Rayleigh–Darcy number vs. solid thickness ratio for $Da = 10^{-3}$.

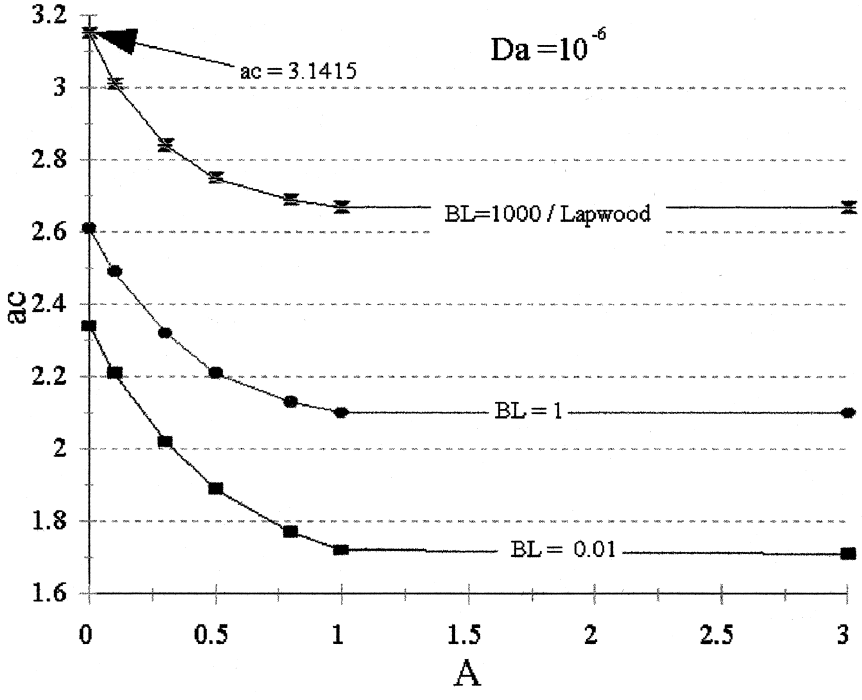

Fig. 5. Critical wave number vs. solid thickness ratio for $Da = 10^{-6}$.

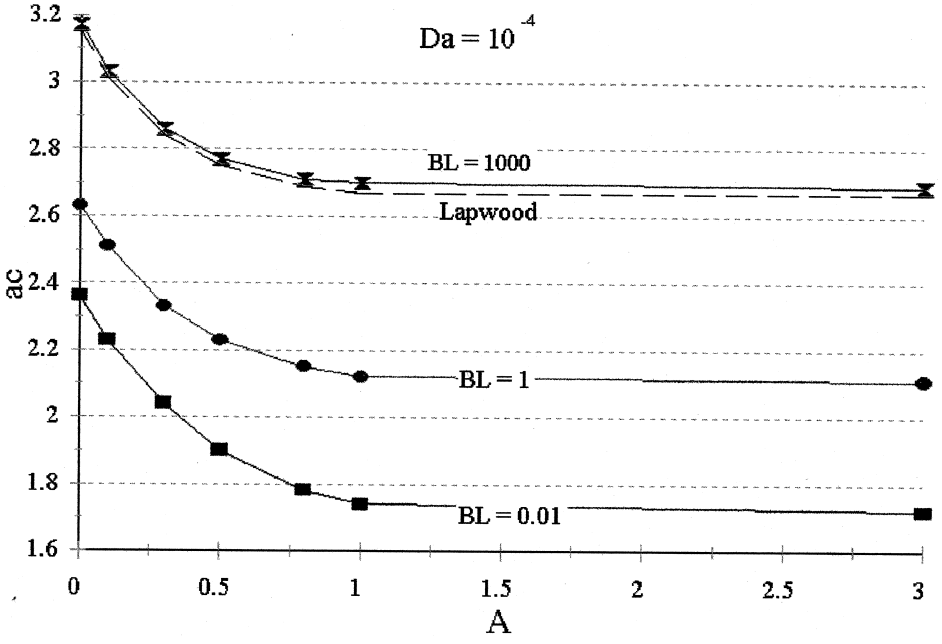

Fig. 6. Critical wave number vs. solid thickness ratio for $Da = 10^{-4}$.

for the less dense case of $Da = 10^{-3}$ (and an isothermal bottom wall), as the solid thickness ratio increases monotonically, the critical Rayleigh number decreases by 6.4%. Such a comparison at two different permeabilities suggests that as the system becomes more dense it is more susceptible to instability, a conclusion that may appear to be counterintuitive at first. However, it should be noted that Fig. 8 presents a plot of the critical Rayleigh–Darcy number as a function of the Darcy number. It shows that the medium will be less stable as its permeability approaches that of a liquid layer. Physically, the liquid layer presents less

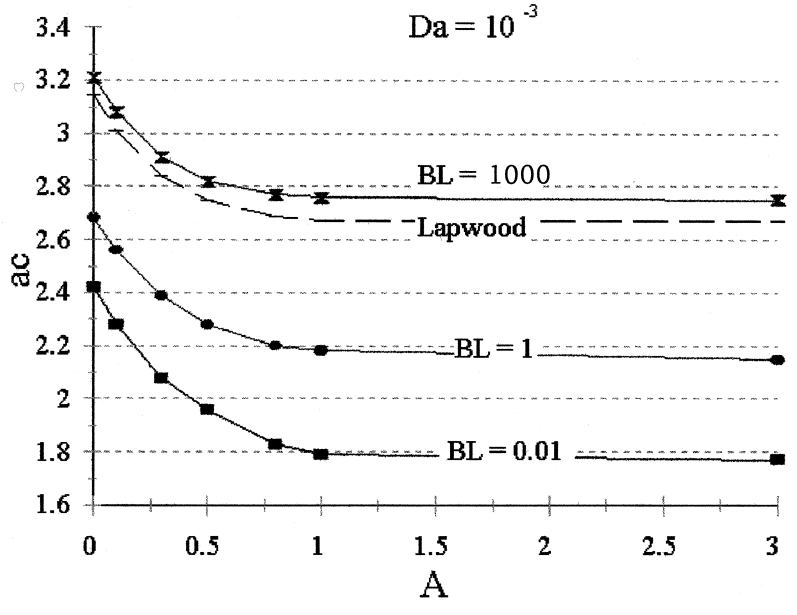

Fig. 7. Critical wave number vs. solid thickness ratio for $Da = 10^{-3}$.

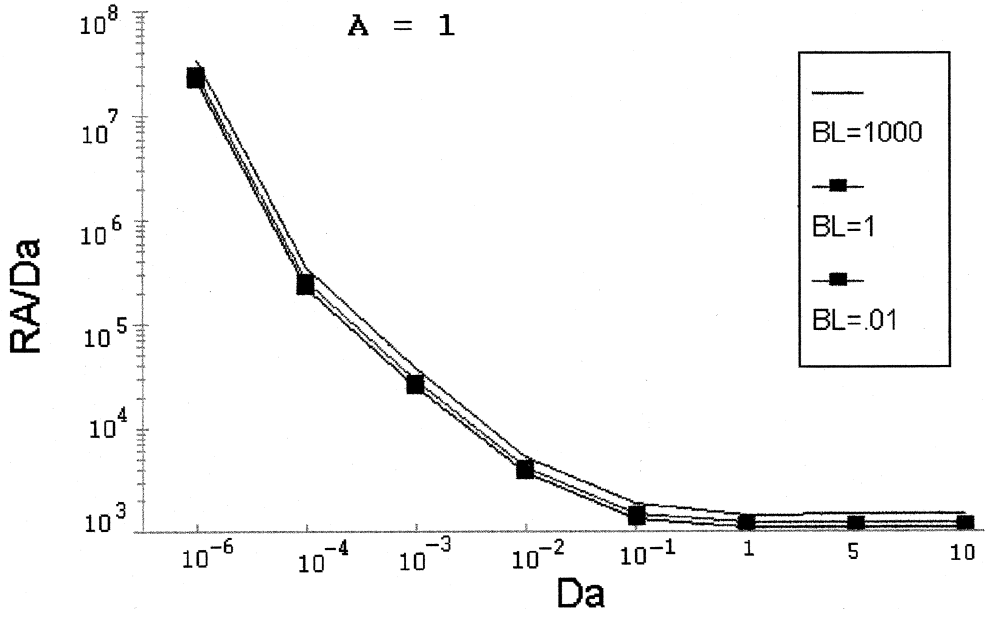

Fig. 8. Critical Rayleigh number vs. Darcy number a variety of boundary conditions ($A=1$).

resistance to the growth and development of an initial disturbance; whereas the porous medium acts to constrict such flow initiation. Thus, as the Darcy number is increased towards the clear liquid limit, non-Darcian effects become more pervasive and the critical conditions deviate more from the predicted limiting values for the porous case. The Brinkman-extended Darcy model employed in this work allows for the comparison between the critical phenomena in a homogeneous liquid vis-à-vis that in a saturated porous layer. Thus, an increase in the amount of solid in the system as well as in the Darcy number of the medium has a destabilizing influence.

The results in Figs. 5–7 indicate that the critical wave numbers tend to become decreased fractions of the critical wave number for the corresponding classical cases as the boundary condition approaches that of an insulated boundary, Theoretically, it is known that in the case of upper and lower insulated boundaries, a vanishing wave number may be assumed. The present results indicate that as the lower boundary becomes less conductive, it acts to constrain the critical wave number as expected from theory. However, in contrast, as the Darcy number increases, the critical wave number tends towards a value that represents a higher fraction of the classical result. Therefore, the largest critical wave number corresponds to a case with maximized Biot (constant temperature boundary) and Darcy numbers. In the Bénard case (pure liquid layer), which may be viewed as the limiting case of a porous medium with an infinite permeability ($Da \gg 0$), the largest critical wave number corresponds to the limiting case of a constant temperature boundary and a minimum solid thickness ($A=0$). In other words, the presence of the porous medium and the solid act to constrain the size of the cell at the onset of convection.

5.2. Effect of fixed boundary conditions

In a typical physical situation the boundary during the process has fixed heat transfer characteristics, usually that of an arbitrarily conducting boundary. By comparing Figs. 2–5, it is noted that decreasing the Biot number or moving towards a constant heat flux boundary has a stabilizing effect on the system (the critical Rayleigh–Darcy number increases).

Figs. 2–4 show the critical Rayleigh–Darcy number, R_{ac}, dependence on the solid thickness for a variety of medium permeabilities for a fixed thermal boundary condition. Fig. 8 also indicates that for all boundary conditions the system is more stable as the medium becomes more dense ($Da \rightarrow 0$), with the constant heat flux boundary among these being the least stable. For $Da \rightarrow 1$, the permeability of the medium may be considered infinite as the difference in critical Rayleigh numbers for this case and the classical Bénard model is negligible. On the other hand, a significant increase in R_c is observed for $Da > 10^{-2}$. This introduces a transition region for values of Da where the medium is too dense to be treated as a bulk liquid and too porous to

model as a porous medium thus introducing non-Darcian behavior [10].

5.3. Solidification of an aluminum preform

The linear stability analysis for the system in this work has two experimentally verifiable physical results: the critical temperature difference for the onset of convection and the corresponding critical wavelength. This analysis has demonstrated, for a range of boundary conditions varying from a constant temperature to a constant heat flux, how the incipient conditions for convection for a pure liquid solidifying in a homogeneous system may be determined. Specific calculations may be performed for a specific system of pure aluminum solidifying in an alumina preform in a gravitational field, possessing the typical parameter values for such aluminum melt systems as [12],

$$\rho_L = 2.39 \times 10^3 \frac{\mathrm{kg}}{\mathrm{m}^3}, \quad k_L = 93 \frac{\mathrm{W}}{\mathrm{m\,K}}, \quad \alpha_L = 37 \times 10^{-6} \frac{\mathrm{m}^2}{\mathrm{s}}$$

$$\mu_L = 1.3 \times 10^{-3}\ \mathrm{Pa \cdot s}, \quad \Delta T_L = 20^\circ\mathrm{C}, \quad T_f = 933.6\ \mathrm{K}$$

$$\beta = 23.1 \times 10^{-6}\ \mathrm{K}^{-1}, \quad L = 0.01\ \mathrm{m}. \tag{47}$$

Fig. 9 indicates that it is possible to establish a relation between the critical Rayleigh numbers based on solid thickness ratio and the medium permeability as determined from the physical properties of the system to the modified Lapwood solution from the theoretical analysis. It is shown that when the temperature difference across the liquid layer is greater than 100 K, the aluminum system is indefinitely unstable compared to the modified Lapwood solution. If the system has a temperature difference of 50 K, the system is unstable depending on the solid thickness ratio. To maintain a stable system other parameters would have to be adjusted to compensate for the effects of the temperature gradient. For the given properties, the system is always stable for a temperature difference of less than 10 K.

6. Closing remarks

The stability analysis performed for a solidifying liquid–saturated porous medium allows calculations of the critical Rayleigh and wave numbers for the incipient convective motion. In the asymptotic limits of $A \to 0$, $Da \to 0$, and $B_L \to \infty$, the critical Rayleigh–

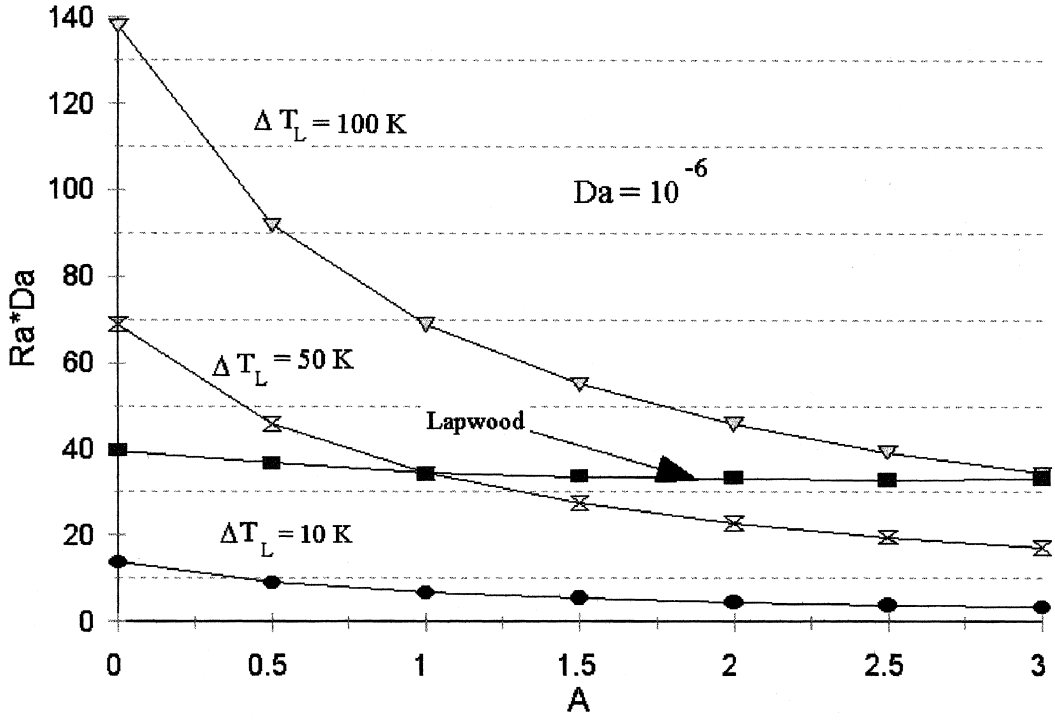

Fig. 9. Critical conditions for the solidification of aluminum for various temperature differences across the liquid layer compared to critical conditions for the modified Lapwood solutions.

Darcy number ($4\pi^2$) and wave number (π) of the classical Lapwood porous medium analysis are recovered from the model examined in this work.

The presence of a solidification boundary acts to destabilize the system. As the solid thickness increases the system becomes less stable as ascertained by a decrease in the Rayleigh number marking the onset of convection. Also, as the solid thickness is increased, the nondimensional wave number decreases, thus rendering smaller convection cells. The number of cells is directly related to the solidification rate and hence the heat transfer rate. As the cell size decreases, a greater heat transfer rate should be expected. The largest wave number corresponds to the case with the highest Biot (constant temperature lower boundary) and Darcy numbers. Furthermore, as the lower boundary condition is modified from an isothermal surface to an insulated boundary, the system becomes less stable.

In comparison to the classical Bénard problem or that of solidification of a pure liquid layer, the presence of the porous medium renders the porous Lapwood model more stable than the bulk liquid analog. As the system becomes more dense or as the permeability decreases, the system becomes more stable. Also it was found that the presence of the porous medium and the solidified layer thickness act to constrain the size of the cell at the onset of convection.

References

[1] S. Chandrasekhar, Hydrodynamic and Hydromagnetic Stability, Dover, New York, 1961.
[2] P.G. Drazin, W.H. Reid, Hydrodynamic Stability, Cambridge University Press, New York, 1981.
[3] E.L. Koschmieder, in: Bénard Cells and Taylor Vortices, Cambridge University Press, New York, 1993, pp. 1–35.
[4] E.R. Lapwood, Convection of a fluid in a porous medium, Proc. Camb. Phil. Soc. 44 (1948) 508–521.
[5] A. Bejan, D.A. Nield, in: Convection in Porous Media, Springer-Verlag, New York, 1992, pp. 8–9, 305.
[6] C. Karcher, U. Müller, Convection in a porous medium with solidification, Fluid Dynamic Research 15 (1995) 25–26.
[7] J.A. Weaver, R. Viskanta, Freezing of liquid-saturated porous media, ASME J. Heat Transfer 108 (1986) 654–659.
[8] C. Beckermann, R. Viskanta, Natural convection solid/liquid phase change in porous media, Int. J. Heat Mass Transfer 31 (1) (1988) 35–46.
[9] S.H. Davis, U. Müller, C. Dietsche, Pattern selection in single-component systems coupling Bénard convection and solidification, J. Fluid Mech. 144 (1984) 133–151.
[10] K.L. Walker, G.M. Homsy, A note on convective instabilities in Boussinesq fluids and porous media, ASME J. Heat Transfer 99 (1977) 338–339.
[11] J.C. Ward, Turbulent flow in porous media 1964, ASCE J. Hydraul. Div. 90 (1964) 6–12.
[12] K.M. Fisher, The effects of fluid flow on the solidification of industrial castings and ingots, Physicochemical Hydrodynamics 2 (1981) 311–326.